Journal of Medicinal Chemistry

pubs.acs.org/jmc Article

Molecular Plasticity of Crystalline CK2α′ Leads to KN2, a Bivalent Inhibitor of Protein Kinase CK2 with Extraordinary Selectivity

Dirk Lindenblatt, Violetta Applegate, Anna Nickelsen, Merlin Klußmann, Ines Neundorf, Claudia Götz, Joachim Jose, and Karsten Niefind*

Cite This: https://doi.org/10.1021/acs.jmedchem.1c00063 Read Online

ACCESS | Metrics & More | Article Recommendations | Supporting Information

ABSTRACT: CK2α and CK2α′ are paralogous catalytic subunits of CK2, which belongs to the eukaryotic protein kinases. CK2 promotes tumorigenesis and the spread of pathogenic viruses like SARS-CoV-2 and is thus an attractive drug target. Efforts to develop selective CK2 inhibitors binding offside the ATP site had disclosed the αD pocket in CK2α; its occupation requires large conformational adaptations of the helix αD. As shown here, the αD pocket is accessible also in CK2α′, where the necessary structural plasticity can be triggered with suitable ligands even in the crystalline state. A CK2α′ structure with an ATP site and an αD pocket ligand guided the design of the bivalent CK2 inhibitor KN2. It binds to CK2 with low nanomolar affinity, is cell-permeable, and suppresses the intracellular phosphorylation of typical CK2 substrates. Kinase profiling revealed a high selectivity of KN2 for CK2 and emphasizes the selectivity-promoting potential of the αD pocket.

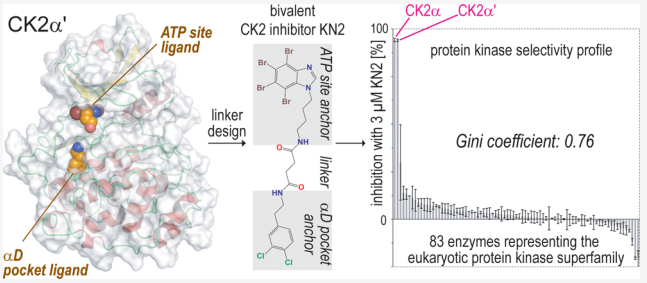

INTRODUCTION

Protein kinase CK2, a member of the superfamily of eukaryotic protein kinases (EPKs), is among several viral and human proteins considered as targets to treat COVID-19[1] as it colocalizes with the nucleocapsid protein of SARS-CoV-2 in filopodia protrusions exploited by the virus for rapid cell-to-cell transfer.[2]

The benefit of CIGB325, an anti-CK2 peptide, in the context of COVID-19 treatment was described recently.[3] A further potential anti-COVID-19 drug is the ATP-competitive CK2 inhibitor CX-4945 (Figure 1a) that was developed for cancer therapy[4] and is subject of clinical studies in the context of COVID-19 (NCT04668209)[5] and cholangiocarcinoma (NCT02128282).[6] CK2 activity is elevated in many cancer tissues; the enzyme promotes cell proliferation and angiogenesis and suppresses apoptosis—three characteristics of cancerogenesis.[7] Upregulated CK2 amplifies tumor-promoting signaling, such as the Wnt, the NF-κB, the PI3K/Akt,[8] or the Hedgehog pathway.[9] In addition, CK2 mediates phosphorylation of caspase recognition sequences and thus protects apoptotic proteins from caspase cleavage. Consequently, CK2 interferes with caspase signaling: its activity inversely correlates with the rate of apoptosis,[10] and tumors develop an undue reliance on CK2 activity to maintain the malignant phenotype.[7]

CX-4945 is a tight-binding CK2 inhibitor (K_i = 223 pM)[11] with antiproliferative activity against a broad panel of cancer cell lines,[4] but its binding to the highly conserved ATP site leads to significant off-target effects: CX-4945 inhibits several other EPKs in the low nanomolar range.[11] Recent efforts resulted in more efficient and selective ATP-competitive CK2 inhibitors,[12−14] but a residual selectivity problem remains as it is inherent to so-called type-I EPK inhibitors[15] that occupy the ATP site in its active conformation.

In many EPKs, this limitation was overcome by addressing the ATP site in an inactive kinase state in which the so-called regulatory (R)-spine is dismantled (type-II inhibitors).[15] The R-spine and its counterpart—the catalytic (C)-spine—are stacks of hydrophobic/aromatic residues (Figure S1) that penetrate the border of the two structural domains of an EPK (Figure 2a).[16] Both spines must be completely established—the C-spine requires the adenine moiety of ATP for this—as a prerequisite of full activity. For CK2, type-II inhibitors are excluded: here, the R-spine is stabilized *via* intramolecular interactions of the N-terminal segment with the helix αC and the activation segment, the canonical regulatory switches in EPKs (Figure 2a).[16] In fact, a dismantled R-spine was never found in any CK2 structure.[17]

Special Issue: New Horizons in Drug Discovery - Understanding and Advancing Kinase Inhibitors

Received: January 14, 2021

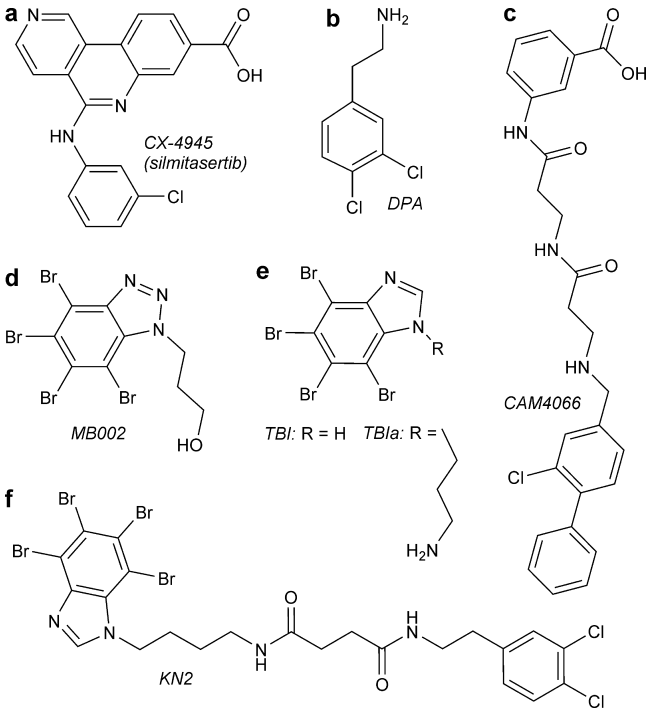

Figure 1. CK2 ligands used or mentioned in this study: (a) CK2 benchmark inhibitor CX-4945;[4] (b) αD pocket ligand 3,4-dichlorophenethylamine (DPA); (c) bivalent inhibitor CAM4066;[24,25] (d) CK2α′ crystallization additive MB002;[34,35] (e) 4,5,6,7-tetrabromo-1*H*-benzo[*d*]imidazol (TBI) and its derivative TBIa, used as a synthon here; and (f) bivalent inhibitor KN2 [N^1-(3,4-dichlorophenethyl)-N^4-(4-(4,5,6,7-tetrabromo-1*H*-benzo[*d*]-imidazol-1-yl)butyl)succinamide] developed in this study.

Instead, CK2 inhibitor design moved toward allosteric compounds[18] (type-IV inhibitors),[19] bisubstrate inhibitors[20−23] or bivalent ligands[24,25] (type-V inhibitors),[19,26] that combine high affinity and selectivity.[27] CK2's quaternary structure with two catalytic subunits (CK2α or CK2α′) bound to a dimer of regulatory chains (CK2β)[28] offers a unique opportunity for this: CK2β antagonistic compounds addressing the CK2β interface of CK2α (Figure 2a) disturb the CK2α/CK2β interaction and the CK2β-dependent enzyme profile.[20,29−33]

A further attractive allosteric site of CK2α is the so-called αD pocket at the back of the canonical helix αD (Figure 2a).[25] Typically in EPKs, the αD pocket is not accessible for small molecules since it is part of the C-spine and filled with a side chain from the helix αD. The latter is therefore largely invariable in its conformation.[16] The helix αD of CK2α, however, is unusually adaptable;[36] depending on its orientation (Figure 2a), it feeds the side chain of either Phe121 or Tyr125 into the C-spine or it unfolds completely and permits access to the αD pocket for ligands such as 3,4-dichlorophenethylamine (DPA; Figure 1b and Figure 2a). This feature of CK2α, found by fragment-based screening,[25] was exploited to design CAM4066, a bivalent inhibitor addressing the ATP site and the αD pocket (Figure 1c).[24,25]

The αD pocket was characterized with human CK2α only.[25] In contrast, the available crystal structures of its paralog CK2α′ suggest conformational invariability in the helix αD region.[35] Therefore, we considered whether CK2α′ can nevertheless provide an accessible αD pocket if an established αD pocket ligand such as DPA (Figure 1b) is offered as the interaction

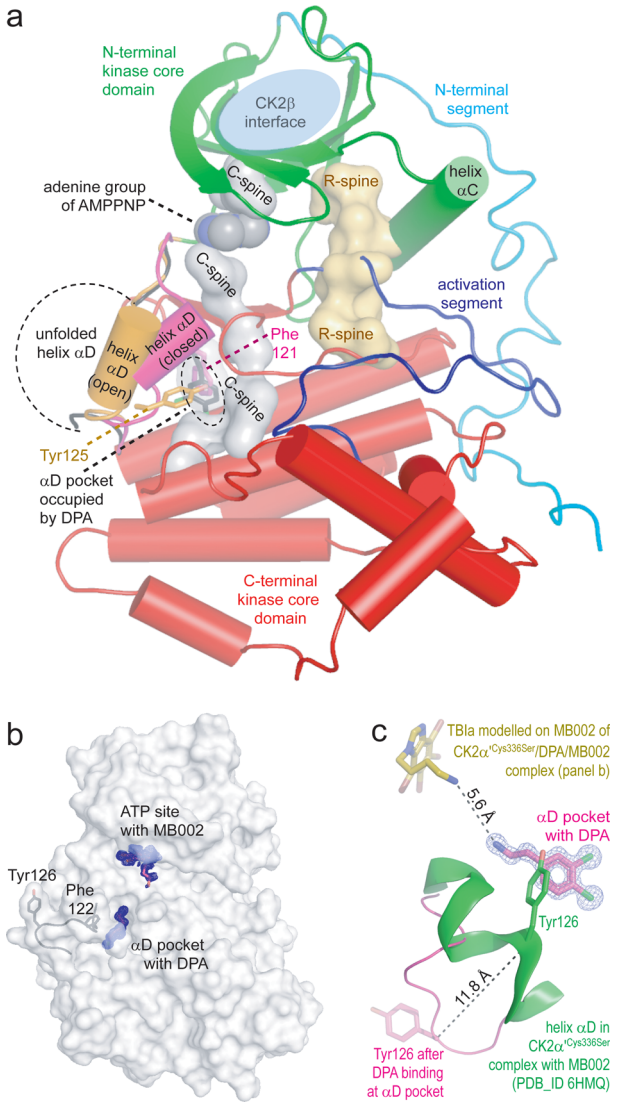

Figure 2. The αD pocket in CK2α/CK2α′. (a) Overview of CK2α with helix αD in closed state (from PDB_ID 3BQC),[36] in open state (from PDB_ID 1PJK),[37] and in unfolded state with αD pocket occupied by DPA (from PDB_ID 5CLP).[25] (b) CK2α′^{Cys336Ser} with bound MB002 and DPA [PDB_ID 7AT9 (Table S1)], both covered with electron density (contour level 1 σ). (c) Helix αD region mobility in crystalline CK2α′^{Cys336Ser} during crystal soaking and starting point of linker design for KN2. Phe121 and Tyr125 of CK2α (panel a) are equivalent to Phe122 and Tyr126 of CK2α′ (panels b,c). The green helix αD (from PDB_ID 6HMQ)[35] marks the initial point of crystal soaking with DPA and the magenta-colored elements from the CK2α′^{Cys336Ser}/DPA/MB002 structure (this work) the end point.

partner. The answer to this question finally led to KN2 (Figure 1f), a bivalent CK2 inhibitor of extremely high selectivity.

RESULTS AND DISCUSSION

DPA Opens the αD Pocket of CK2α′ in the Crystalline State. A further motivation of this work had a methodical background: to combine DPA (Figure 1b) with CK2α′, we used a crystallographic procedure originally developed to solve atomic resolution structures of CK2α′ with ATP-competitive CK2 inhibitors. It depends on crystals of the oxidation-stable mutant CK2α′^{Cys336Ser} (Figure S1) in complex with the ATP site ligand MB002 (Figure 1d)[34] that is subsequently

https://doi.org/10.1021/acs.jmedchem.1c00063
J. Med. Chem. XXXX, XXX, XXX−XXX

Scheme 1. Synthesis of KN2[a]

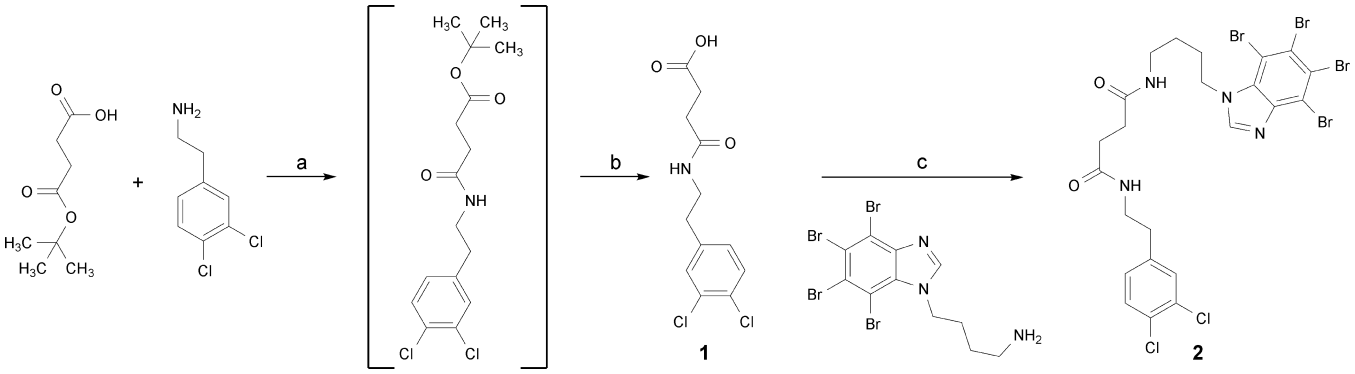

[a]Reagents and conditions: (a) DIPEA, HATU, DMF, 24 h, rt; (b) TIPS, DCM/TFA, 2 h, rt, 74%; (c) DIPEA, HATU, DMF, 24 h, rt, 66%.

exchanged by extensive soaking.[35] The method was successful with CX-4945 and with several other high-, medium-, and low-affinity ATP-competitive ligands,[35,38,39] but it was unclear if it works for allosteric sites, as well. A first study to explore this failed insofar as it proved that certain 2-aminothiazole compounds described before to be allosteric CK2 inhibitors[40] actually bind to the ATP site.[38]

The use of DPA was a further attempt, and here, the procedure, in fact, resulted in a high-resolution ternary complex structure of CK2$\alpha'^{Cys336Ser}$, MB002, and DPA (Table S1), in which the latter occupied the allosteric αD pocket while the ATP site and its MB002 ligand were largely unaffected (Figure 2b). A comparison of this structure with the starting point of the soaking procedure—represented by a CK2$\alpha'^{Cys336Ser}$/MB002 structure (PDB_ID 6HMQ)[35]—reveals that the occupation of the αD pocket by DPA required a movement of the helix αD region by around 12 Å combined with a loss of the helical geometry (Figure 2c and Movie S1).

Noteworthy, this huge displacement happened within the crystal during soaking. Hence, CK2α' not only is able to emulate its paralog CK2α in opening of the αD pocket but also provides a remarkable example of molecular plasticity of a crystalline protein. Apparently, the ATP site and the αD pocket of CK2$\alpha'^{Cys336Ser}$ in this crystalline environment can be independently addressed by soaking of suitable compounds. For the future, this suggests a path to atomic resolution structures of ternary CK2$\alpha'^{Cys336Ser}$ complexes with various couples of ATP site and αD pocket ligands.

Design, Synthesis, and Inhibitory Efficacy of the Bivalent CK2 Inhibitor KN2. The ternary complex structure in Figure 2b inspired us to connect the two ligands and provided a perfect basis to model a tailored linker. The linker design in CAM4066 had demonstrated the benefit of peptide groups to improve solubility in an aqueous environment and to combine the potential to form hydrogen bonds with a balanced degree of flexibility.[24] To adapt this strategy, we used two terminal synthons with amino groups, namely, DPA itself (Figure 1b) and TBIa[41] (Figure 1e) that resembles MB002. After TBIa was modeled into the ternary CK2$\alpha'^{Cys336Ser}$/DPA/MB002 complex (Figure 2b) by replacing MB002 (Figure 2c), the two amino groups were only 5.6 Å apart from each other, suggesting succinic acid as a dicarbonic acid with a perfect length to bridge this distance and to form two peptide bonds. Unlike CX-4945 (Figure 1a) and CAM4066 (Figure 1c), the resulting compound KN2 (Figure 1f) did not contain a negative charge that could enforce a pro-drug approach to achieve membrane penetration as reported for CAM4066.[25] A topological polar surface area of 76.02 Å^2 and a lipophilicity value (clogP) of 6.38 were calculated with SwissADME.[42] The latter is larger than recommended,[43] but overall *in silico* evaluation did not exclude cell permeability; rather, it suggested to proceed with KN2 as a promising candidate for a bivalent CK2 inhibitor *in vitro* and in the cell.

After synthesis of KN2 according to Scheme 1, its CK2 inhibitory efficacy was tested using tetrameric CK2 holoenzymes based on either CK2α or CK2$\alpha'^{Cys336Ser}$ (Figure 3a). At 100 μM ATP, the IC_{50} values were 19.3 ± 6.4 nM with the CK2$\alpha_2\beta_2$ isoform and 15.6 ± 5.5 nM with the CK2$\alpha'_2\beta_2$ isoform, corresponding to K_i values of 6.1 ± 2.0 nM (CK2$\alpha_2\beta_2$) and 4.0 ± 1.4 nM (CK2$\alpha'_2\beta_2$). Thus, the affinity of KN2 to the enzyme is between those of CX-4945 (K_i = 0.223 nM with CK2$\alpha_2\beta_2$)[11] and CAM4066 (IC_{50} = 370 nM at 25 μM ATP with CK2α)[25] and significantly higher than the affinity of TBIa (Figure 1e), KN2's synthon at the side of the ATP cavity (K_i = 190 nM with CK2$\alpha_2\beta_2$).[41] Overall, these data indicate a very strong binding of KN2 to both CK2α paralogs.

To explore if KN2 inhibits CK2 within the cell, we first applied a toxicity assay to check if it is cell-permeable enough to affect whole cells. For this, HeLa cells, a tumor cell line relying on high levels of CK2, were chosen and for comparison HEK293 cells, an artificially immortalized nontumor cell line being less sensitive toward CK2 inhibitors.[7,32] In fact, KN2 proved to be cell-permeable and cytotoxic (Figure 3b). The EC_{50} value is significantly (p-value 0.0198) lower for HeLa cells (6.19 μM) than for HEK293 cells (15.94 μM), consistent with their higher CK2 requirement for viability. CX-4945 was somewhat more cytotoxic for HeLa cells than KN2 (Figure 3c); the EC_{50} value we determined (2.10 μM) is in the same range as reported for a panel of 13 cancer cell lines.[44] We did not detect any CX-4945 cytotoxicity with HEK293 cells up to a concentration of 100 μM (Figure 3c). This finding is consistent with the results of a caspase 3/7 activation assay with CX-4945 reported earlier.[4]

Within cells, CK2 regulates the PI3K/Akt signaling pathway among others *via* phosphorylation of Akt/PKB kinase.[8] The major CK2 phosphorylation site is Ser129,[8] and the down-regulation of the Akt phosphorylation at Ser129 indicates reliably that an inhibitor affects CK2 intracellularly.[4] In Western blot analyses, the phosphorylation signal of Akt at Ser129 vanished in a concentration- and time-dependent manner for both cell lines (Figure 3c,d). In summary, KN2 can

https://doi.org/10.1021/acs.jmedchem.1c00063
J. Med. Chem. XXXX, XXX, XXX−XXX

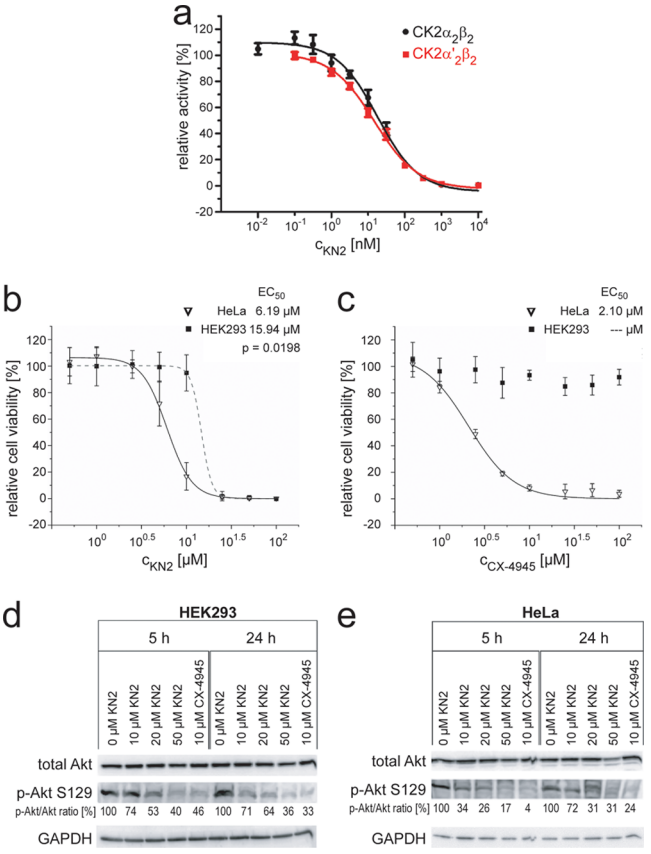

Figure 3. Functional characterization of KN2. (a) Inhibition of CK2α- and CK2α'-based CK2 holoenzymes (quadruple measurements). (b,c) Cytotoxic effect of KN2 (b) and for comparison CX-4945 (c) on HeLa and HEK293 cells (experiments performed as triplicates). (d,e) Western blot analysis of HEK293 (d) and HeLa cells (e) to explore the effect of KN2 on the CK2-dependent phosphorylation level of AKT/PKB at Ser129.

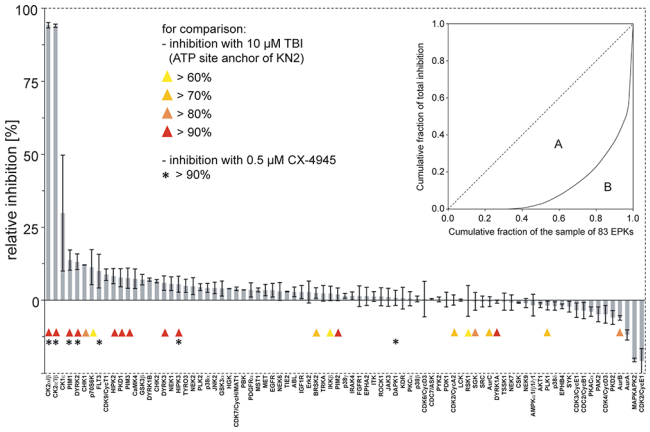

Figure 4. Selectivity screening of KN2 (3 μM) against 83 different EPKs from all families of the human kinome. Error bars correspond to standard deviation (±) based on duplicate measurements (details in Table S2). Color-coded bars plus triangles indicate EPKs inhibited by 10 μM TBI (Figure 1e) according to Pagano *et al.*[45] Asterisks mark EPKs inhibited by 0.5 μM CX-4945 (Figure 1a) to at least 90% as published by Battistutta *et al.*[11] The inset shows the Lorentzian curve derived from the KN2 selectivity profile according to Graczyk[46] for calculation of the Gini coefficient; the latter equals the area ratio A/(A + B).

enter cells and manipulate the cellular CK2-dependent phosphoproteome.

KN2 Is Highly Selective for CK2α and CK2α'. CAM4066 (Figure 1c) was designed with the aim of a high selectivity by exploiting the αD pocket.[25] To avoid that the ATP site anchor group dominates binding, CAM4066 was supplied only with a low-affinity anchor there.[25] In the case of KN2, we did not adapt this precautionary strategy, but we were interested if high selectivity can be achieved on the basis of a high-affinity ATP site fragment, as well. To explore this quantitatively, KN2 was tested against a panel of 83 EPKs from all families of the human kinome including those reported to be off-targets of CK2 inhibitors (Table S2). In the screening, the ATP concentration was in the range of the K_M of the respective kinase. Throughout, a KN2 concentration of 3 μM was applied, which equals approximately 150−200 times the IC_{50} value with respect to CK2. With such a high concentration, even weak off-target effects should be reliably detected. The resulting $c_{inhibitor}/IC_{50}$ ratio is close to the range Graczyk[46] recommended for the application of the Gini coefficient as a numerical expression of selectivity.

Under these conditions, KN2 inhibited CK2α and CK2α' to about 94% (Figure 4 and Table S3). The only apparent off-target was CK1ε with an inhibition of 29.9%, however with a high standard deviation of ±19.84% (Figure 4 and Table S3). To explore its putative interaction with KN2, we determined a cocrystal structure of KN2 with the close CK1ε-relative CK1δ (sequence identity 97.3% and no sequence differences in the region of the ATP site and the αD pocket; Table S2). In this structure, a KN2 ligand is only weakly visible at the ATP site, but neither an open helix αD conformation nor an accessible αD pocket could be observed (Figure S2). Final clarity was provided by a dose−response curve (Figure S3), demonstrating that KN2 is only a negligible CK1ε inhibitor (IC_{50} value more than 30 μM).

Notably, 3 μM KN2 did not inhibit a number of EPKs previously reported to be significantly affected by CX-4945 at 0.5 μM[11] and by TBI at 10 μM[45] (colors and asterisks in Figure 4). Rigorous selectivity comparisons would require K_i values, which are independent of ATP and inhibitor concentrations. Their determination is laborious, so instead, the Gini coefficient calculated from selectivity profile data was introduced as a quantitative indicator of kinase selectivity.[46] Its use is recommended now,[47] and it was applied for several CK2 inhibitors, among them CX-4945[11] and CAM4066.[25] A Gini coefficient of 0.76, calculated from the kinase profile in Figure 4, suggests an extraordinary high selectivity of KN2. For comparison, the selectivity data published for 10 μM of KN2's ATP-site anchor TBI[45] lead to a Gini coefficient of 0.30, whereas data from the same article[45] for 1 μM 4,5,6,7-tetrabromo-1*H*-benzo[*d*][1,2,3]triazole—the mother compound of MB002 (Figure 1d)—correspond to a Gini coefficient of 0.68. The Gini coefficient published for CAM4066 is slightly higher than that of KN2 (0.82), but it was calculated on the basis of a smaller panel (52 EPKs) and a lower inhibitor concentration (2 μM).[25] For CX-4945, a Gini coefficient of 0.62 was reported, determined with 102 EPKs and an inhibitor concentration of 0.5 μM.[11] Overall, the high Gini coefficient of KN2 suggests that it mimics the binding mode of CAM4066 by exploiting the αD pocket in favor of selectivity.

KN2 Binding to CK2α and CK2α' Benefits from the Tailor-Made Linker. To investigate the binding mode

https://doi.org/10.1021/acs.jmedchem.1c00063
J. Med. Chem. XXXX, XXX, XXX−XXX

precisely, we determined crystal structures of KN2 in complex with CK2$\alpha'^{Cys336Ser}$ and CK2α^{1-335} (Table S1). In both cases, crystal soaking was applied and started with DPA (Figure 1b) plus the intention to open the αD pocket first in order to assist the binding of KN2. Significantly, however, this strategy turned out to be unnecessary: irrespective of the presence and the concentration of DPA, KN2 diffused smoothly into CK2$\alpha'^{Cys336Ser}$ or CK2α^{1-335} crystals, induced access to the αD pocket there (Movie S2) and was finally well-defined by electron densities (with atomic resolution in case of the CK2$\alpha'^{Cys336Ser}$/KN2 complex) (Figure 5a).

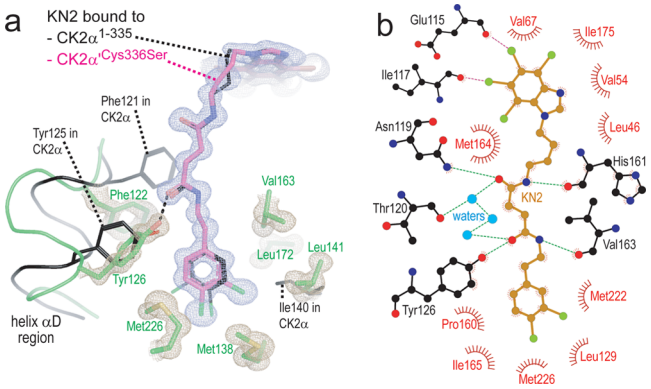

Figure 5. KN2 binding to CK2α/CK2α'. (a) KN2 and parts of its protein environment in complex with CK2$\alpha'^{Cys336Ser}$ covered by electron density (contouring level 1.5 σ); for comparison, parts of the CK2α^{1-335}/KN2 complex were drawn (C atoms in black; Phe121, Tyr125, and Ile140 of CK2α are equivalent to Phe122, Tyr126, and Leu141 of CK2α'); crystallographic details are given in Table S1. (b) LIGPLOT[51] projection of KN2 bound to CK2$\alpha'^{Cys336Ser}$. Green dotted lines, H-bonds; red dotted lines, halogen bonds.

The binding of KN2 is essentially as anticipated by *in silico* modeling. The four bromo substituents participate *via* halogen bonds and hydrophobic interactions (Figure 5b), as well-known for TBI derivatives.[48] As intended, the two peptide groups of the linker contribute to affinity by a number of hydrogen bonds with the protein matrix (Figure 5b). One of these H-bonds is formed with the terminal hydroxy group of Tyr126 (Tyr125 in CK2α); this means that the helix αD region, which is largely disordered in the published CK2α/DPA structure[25] (Figure 2a) and in the CK2$\alpha'^{Cys336Ser}$/DPA/MB002 complex structure of this work (Figure 2b), reassembles within the crystal when the high-affinity ligand KN2 is bound (Movie S2).

Surprisingly, the orientation of the αD pocket anchor in the CK2α^{1-335}/KN2 complex differs from the CK2$\alpha'^{Cys336Ser}$/KN2 complex (Figure 5a) due to space restrictions in the αD pocket enforced by the terminal methyl group of Ile140. In the future, this and other subtle differences between CK2α and CK2α' in the αD pocket region may assist attempts to develop inhibitors discriminating between both paralogs.[35,49,50]

Efforts to further improve the selectivity and affinity of KN2 plus other properties essential for a drug can include the linker region and the ATP site, as well. For such intentions, an excellent basis is provided not only by the complex structures of this work but also by the option to replace the MB002 ligand of CK2$\alpha'^{Cys336Ser}$/DPA/MB002 crystals by other ATP-competitive compounds and thus to determine further atomic resolution structures of ternary CK2$\alpha'^{Cys336Ser}$ complexes. Whether follow-up compounds of KN2 resulting from such efforts can improve COVID-19 or cancer therapies is a particularly interesting question for future studies.

CONCLUSION

Allosteric binding sites play an increasing role in protein kinase inhibitor design to escape the limitations of the ATP site with respect to selectivity.[15,19,26,27] The αD pocket of CK2α and its paralog CK2α'—the result of a local helix αD plasticity unique among eukaryotic protein kinases—is such an allosteric site. Its potential was known from the proof-of-concept inhibitor CAM4066[24,25] and was emphasized here again with the bivalent CK2 inhibitor KN2. In KN2, a high-affinity, but low-selectivity, ATP-competitive inhibitor was coupled to a low-affinity, but selectivity providing ligand of the αD pocket *via* a tailor-made linker. The basis for the linker design was an atomic resolution CK2α' structure in complex with an ATP site and an αD pocket fragment. It was provided by a crystallographic approach exploiting the plasticity of helix αD in crystalline CK2α'. This procedure is potentially applicable to determine CK2α' complex structures with various combinations of ATP site and αD pocket ligands. This would be particularly valuable if a recent prediction that bivalent ligands constitute the next generation of CK2 inhibitors should come true.[27]

EXPERIMENTAL SECTION

Chemicals. 3,4-Dichlorophenethylamine (DPA; Figure 1b), succinic acid, and chemicals in general were purchased from Sigma-Aldrich. 3-(4,5,6,7-Tetrabromo-1*H*-benzotriazol-1-yl)propan-1-ol (MB002; Figure 1d)[52] and 4-(4,5,6,7-tetrabromo-1*H*-benzo[*d*]-imidazol-1-yl)butan-1-amine (TBIa; Figure 1e)[41] were kind gifts from the group of Professor Maria Bretner, Warsaw, Poland. TBIa was used as a synthon for KN2 here; its synthesis and analytical characterization was described in detail by Chojnacki *et al.*[41]

Analytical Chemistry. A ^{1}H NMR spectrum of the coupling product between succinic acid and DPA (compound **1**) was measured on a Bruker Avance I 300 spectrometer (300 MHz). The residual protonated solvent signal of DMSO-d_6 served as an internal reference.

NMR spectra of KN2 were recorded at 26.0 °C in deuterated solvents on an Agilent DD2 600 MHz spectrometer equipped with a cold probe (Agilent, Santa Clara, CA, USA). Chemical shifts (δ) are reported in parts per million (ppm) against the reference substance tetramethylsilane and calculated using the solvent residual peak of the undeuterated solvent. The assignment of ^{1}H and ^{13}C NMR signals were supported by gCOSY, gHSQC, gHMBC, and bsgHMBC spectra (not shown). The data were analyzed using MestReNova 12.0.4 (Mestrelab, Santiago de Compostela, Spain).

An LTQ XL three-segment 2D linear ion trap mass spectrometer (Thermo Fisher Scientific) was used to acquire mass spectra of the coupling product between succinic acid and DPA (compound **1**). The sample was injected by a 1260 infinity autosampler (Agilent) with an injection volume of 10 μL and ionized by an electrospray ionization source. The measurement was conducted with a spray voltage of 4.5 keV, a N_2 sheath gas pressure of 6.5 × 10^5 Pa, a capillary voltage of 44 V, and a capillary temperature of 275 °C. An Aeris 3.6 μm peptide XB-C18 (150 × 4.6 mm) (Phenomenex) LC column was used for compound separation. A linear ACN gradient, 50−100% ACN over 15 min, was applied with water containing 0.1% formic acid (A) and ACN containing 0.08% formic acid (B). The flow rate was set to 0.6 mL/min.

For the confirmation of the KN2 sum formula, a flow injection analysis coupled to a mass spectrometer (FIA-MS) was used. The LC system consisted of an Ultimate 3000 RS Dionex system (Dionex Softron, Germering, Germany) with DGP-3600RS pump and WPS-3000RS rapid separation autosampler. The high-resolution mass

https://doi.org/10.1021/acs.jmedchem.1c00063
J. Med. Chem. XXXX, XXX, XXX−XXX

spectrometer was a MicrOTOF-Q II (Bruker Daltonics, Bremen, Germany) with ESI interface (Bruker Daltonics, Bremen, Germany). The mobile phase of the LC system consisted of acetonitrile/ammonium formate [10 mM]/formic acid 50:50:0.1 (v/v/v) with a flow of 0.1 mL/min. The electrospray ion source was operated in positive ionization mode, scan range of 120−800 m/z. The capillary was set to ±4.5 kV; the nebulizer was operated at 0.4 bar, and the dry gas was set to 4 L/min at a temperature of 180 °C. Transfer voltages: funnels 1 and 2 were set to 200 Vpp. The hexapole RF voltage was set to 100 Vpp. The transfer time was adapted to 70 μs. Mass calibration was done using a 20 mM sodium formate solution.

4-((2-(3,4-Dichlorophenyl)ethyl)amino)-4-oxobutanoic acid (Compound 1). 4-(*tert*-Butoxy)-4-oxobutanoic acid (130 mg, 0.75 mmol 1.00 equiv) was dissolved in DMF (5 mL) and mixed with DIPEA (520 μL, 2.99 mmol, 3.99 equiv). Subsequently, HATU (380 mg, 1 mmol, 1.33 equiv) was added to this solution. The mixture was stirred at room temperature for 20 min. DPA (Figure 1b; 179 mg, 0.95 mmol, 1.27 equiv) was then added to the reaction solution. After being stirred for 24 h, the solution was diluted with ice-cold water (25 mL). The product was extracted with DCM (3 × 15 mL). The combined organic layers were concentrated to dryness *in vacuo*. The residue was again dissolved in a mixture of DCM (5 mL) and triisopropylsilane (0.15 mL, 0.73 mmol, 0.97 equiv). The *tert*-butyl protection group was cleaved for 2 h by adding trifluoroacetic acid (5 mL), followed by neutralization with solid Na_2HCO_3. The solution was mixed with half-saturated Na_2HCO_3 (50 mL) and washed with cyclohexane (3 × 30 mL) and DCM (3 × 30 mL). The aqueous layers were collected and acidified with HCl. Purification of the precipitate was performed *via* preparative reversed-phase HPLC (C18 column, ACN gradient: 10−60% with 0.1% TFA, 6.0 mL/min). Compound **1** (4-((2-(3,4-dichlorophenyl)ethyl)amino)-4-oxobutanoic acid) crystallized as colorless needles (162 mg, 0.56 mmol, 74% yield). ^{1}H NMR (300 MHz, DMSO-d_6, Figure S4): δ (ppm) = 12.04 (br, 1H), 7.91 (t, J = 5.5 Hz, 1H), 7.51 (d, J = 8.1 Hz, 1H), 7.50 (d, J = 2.0 Hz, 1H), 7.20 (dd, J = 2.0, 8.2 Hz, 1H), 3.26 (d, J = 5.9 Hz, 1H), 2.70 (t, J = 6.9 Hz, 2H), 2.50 (quint, J = 3.6 Hz, DMSO), 2.39 (t, J = 6.2 Hz, 2H), 2.29 (t, J = 6.5 Hz, 2H). MS (ESI) m/z calcd for $C_{12}H_{13}Cl_2NO_3$ $[M + H]^+$ 290.03; found 290.10.

(N^1-(3,4-Dichlorophenethyl)-N^4-(4-(4,5,6,7-tetrabromo-1*H*-benzo[*d*]imidazol-1-yl)butyl)succinamide) (Compound 2, KN2). For a second coupling step, 4-((2-(3,4-dichlorophenyl)ethyl)-amino)-4-oxobutanoic acid (25 mg, 86 μmol, 1.00 equiv) was dissolved in DMF (2 mL) and mixed with DIPEA (120 μL, 0.69 mmol, 8.02 equiv). The mixture was preincubated for 20 min after HATU (42.6 mg, 112 μmol, 1.30 equiv) was added. Then, 4-(4,5,6,7-tetrabromo-1*H*-benzimidazol-1-yl)butan-1-amine (TBIa, Figure 1e; 41 mg, 81 μmol, 0.94 equiv) was added, and the mixture was stirred for 24 h at room temperature. Subsequently, 20 mL of DCM was added, and the product was washed with water (3 × 50 mL). The final purification of KN2 was performed by preparative reversed-phase HPLC (Hitachi) using a VP250/16 Nucleodur 100-5 C18ec column (Macherey-Nagel) and an ACN gradient (50−90% with 0.1% TFA; 6.0 mL/min; Figure S5). KN2 was concentrated to dryness *in vacuo* using an Xcel/Vap (Horizon Technology) to isolate the product as colorless solid (44 mg, 57 μmol, 66% yield). The purity is 97.1% according to the integrated HPLC trace (retention time 9.17 min; Figure S5). ^{1}H NMR (600 MHz, DMSO-d_6, Figure S6): δ (ppm) = 8.49 (s, 1H), 7.86 (t, J = 5.6 Hz, 1H), 7.81 (t, J = 5.7 Hz, 1H), 7.50 (d, J = 8.2 Hz, 1H), 7.44 (d, J = 2.0 Hz, 1H), 7.15 (dd, J = 8.2, 2.0 Hz, 1H), 4.49 (t, J = 7.3 Hz, 2H), 3.24−3.20 (m, 2H), 3.08−3.03 (m, 2H), 2.65 (t, J = 7.0 Hz, 2H), 2.50 (quint, J = 3.6 Hz, DMSO), 2.24 (s, 4H), 1.82−1.74 (m, 2H), 1.41−1.34 (m, 2H). ^{13}C NMR (151 MHz, DMSO-d_6, Figure S7): δ (ppm) = 171.3 (1C), 171.2 (1C), 148.9 (1C), 143.7 (1C), 140.9 (1C), 131.3 (1C), 130.7 (2C), 130.2 (1C), 129.2 (1C), 128.6 (1C), 122.4 (1C), 120.4 (1C), 116.6 (1C), 106.6 (1C), 46.1 (1C), 39.6 (1C), 39.5 (DMSO), 37.8 (1C), 34.0 (1C), 30.73 (1C), 30.71 (1C), 29.0 (1C), 26.0 (1C). HRMS m/z calcd for $C_{23}H_{22}Br_4Cl_2N_4O_2$ $[M + H]^+$ 772.7926; found 772.7894 (Figure S8).

Protein Expression and Purification. For the purpose of crystallization, CK2α^{1-335}, a C-terminal deletion mutant of human CK2α,[37] and CK2$\alpha'^{Cys336Ser}$, a point mutant of human CK2α',[34] without the problem of forming intermolecular disulfide bonds under oxidative conditions,[53] were used. Both constructs were prepared as described previously.[35]

The enzyme kinetic measurements were performed with heterotetrameric CK2 holoenzyme constructs, namely, with $(CK2\alpha)_2(CK2\beta^{1-193})_2$ and with $(CK2\alpha'^{Cys336Ser})_2(CK2\beta^{1-193})_2$. The latter was prepared as described,[35] whereas the $(CK2\alpha)_2(CK2\beta^{1-193})_2$ holoenzyme was produced as follows: full-length CK2α and CK2β^{1-193} were separately expressed in *Escherichia coli* BL21(DE3) using a pT7-7 plasmid system. Bacterial cells were transformed and cultured overnight in lysogeny broth at 37 °C with 200 rpm shaking. Cells were then grown in 1 L phosphate medium[35] to an OD_{578} of 0.5. Protein expression was induced by the addition of isopropyl β-D-1-thiogalactopyranoside to a final concentration of 1 mM. After an incubation of 4 h at 30 °C and 200 rpm shaking, the cells were harvested, mixed in equal amounts, and suspended in lysis buffer (300 mM NaCl, 1.3 mg/mL lysozyme, 13 μg/mL DNase I, 25 mM Tris/HCl, pH 8.5). After 30 min incubation on ice, the cells were disrupted by sonification (6 × 30 s on ice) and the cell lysate was clarified by centrifugation (100.000g, 4 °C, 1 h) to remove cell debris. The supernatant was applied to a phosphocellulose column and afterward to a HiTrap heparin HP column (GE Healthcare, Buckinghamshire, UK) for purification according to Raaf *et al.*[36] An analytical size exclusion step with a Superdex 200 column (GE Healthcare, Buckinghamshire, UK; running buffer containing 1 M NaCl, 25 mM Tris/HCl, pH 8.5) was attached to exclude the presence of free catalytic subunit.

Enzyme Kinetics. The reduction of CK2 phosphorylation activity by KN2 (Figure 3a) was analyzed with a nonradioactive method based on capillary electrophoresis (CE),[54] where the extent of CK2 substrate peptide (RRRDDDSDDD) phosphorylation was determined by CE with a UV detector at 195 nm. The background electrolyte of the CE runs was 2 M acetic acid (pH 2) at a current of 30 μA.

Inhibitor solutions in dimethyl sulfoxide (DMSO) covering a concentration range from 0.001 to 100 μM were prepared. Enzyme solutions containing 0.25 μg of $(CK2\alpha)_2(CK2\beta^{1-193})_2$ or $(CK2\alpha'^{Cys336Ser})_2(CK2\beta^{1-193})_2$ in 100 mM NaCl, 10 mM $MgCl_2$, 50 mM Tris/HCl, pH 7.5, were supplemented with 2 μL of inhibitor solution to a final volume of 80 μL. The mixture was preincubated for 10 min at 37 °C with continuous shaking at 300 rpm. Kinase reaction was started by addition of a 120 μL solution of 190 μM CK2 substrate peptide RRRDDDSDDD and 100 μM cosubstrate ATP in 150 mM NaCl, 5 mM $MgCl_2$, 25 mM Tris/HCl, pH 8.5. After an incubation time of 3 min (CK2α-based holoenzyme) or 7 min (CK2α'-based holoenzyme) at 37 °C with continuous shaking at 300 rpm, the reaction was stopped by addition of 5 μL of 0.5 M EDTA and by cooling on ice. In this time, 10% of the substrate was usually phosphorylated in the absence of KN2.

The reactions were performed as independent quadruples, and reactions with 2 μL of DMSO without inhibitor served as a control (100% activity). Relative inhibition was calculated as inhibition [%] = (1 − sample/100% activity) × 100. The IC_{50} values were determined from the midpoint of a sigmoidal curve [equation: Y = bottom + (top − bottom)/(1 + 10^((LogIC$_{50}$ − X) × HillSlope)), fitted by GraphPad Prism (GraphPad, La Jolla, CA, USA)]. K_i values of KN2 were calculated according to the equation of tight-binding inhibition: $IC_{50} = K_i(1 + [ATP]/K_{M,ATP}) + [enzyme]/2$,[55] assuming competitive inhibition with respect to ATP. For this, a $K_{M,ATP}$ value of 81.6 ± 0.2 μM as determined by Pietsch *et al.*[20] was applied.

The inhibition of human CK1ε by KN2 (Figure S3) was quantified by Carna Bioscience, Inc., Kobe, Japan. The catalytic domain of human CK1ε (residues 1−348) as a GST-fusion construct was used for the experiments performed at room temperature, pH 7.5, and with an ATP concentration of 25 μM. Ten different KN2 concentrations from 1 nM to 30 μM were tested; each data point was measured twice.

https://doi.org/10.1021/acs.jmedchem.1c00063
J. Med. Chem. XXXX, XXX, XXX−XXX

Cell Toxicity Assay. To determine the cytotoxic effects of KN2 and for comparison CX-4945 (free acid; purchased from SelleckChem, Munich, Germany) toward HeLa cells (ATCC: CCL-2) and HEK293 cells (ATCC: CRL-1573), the cells were seeded (HeLa: 1.4×10^4; HEK293: 3.7×10^4) in a 96-well plate and grown overnight in media (HeLa: RPMI-1640 culture medium supplemented with 4 mM L-glutamine and 10% fetal bovine serum (FBS); HEK293: minimum essential medium Eagle supplemented with 4 mM L-glutamine and 15% FBS) to 70−80% confluency at 37 °C, 5% CO_2, and increased air humidity. On the next day, cells were incubated with different dilutions of KN2 or CX-4945, which were prepared in the appropriate serum-free medium. After 24 h, cells were washed with phosphate-buffered saline except for the positive control, which was treated with 70% ethanol for 10 min. Cell viability was determined using a resazurin-based cytotoxicity assay (Sigma-Aldrich), in which the conversion of resazurin to resorufin by metabolizing cells can be monitored at 595 nm (λ_{ex} = 550 nm). Cells were incubated for 1−2 h with a 1:10 dilution of a resazurin solution in serum-free medium (v/v) at 37 °C, 5% CO_2, and humidified atmosphere. The resulting fluorescence of the metabolized product was monitored using a Tecan infinite M200 plate reader. All assays were performed as triplicates. The *p*-value given in Figure 3b was calculated with an unpaired *t* test using Microsoft Excel.

Western Blot Analysis of Intracellular CK2 Phosphorylation. The human cell lines HEK293 (ATCC: CRL-1573) and HeLa (ATCC: CCL-2) were cultured in Dulbecco's modified Eagle's medium (DMEM) (Invitrogen GmbH, Karlsruhe, Germany) supplemented with 10% FBS at 37 °C in an atmosphere enriched with 5% CO_2. Cells were seeded in 60 mm cell culture dishes the day before treatment. Ten millimolar stock solutions of the CK2 inhibitors KN2 and CX-4945 (free acid; purchased from SelleckChem, Munich, Germany), each dissolved in dimethyl sulfoxide (Merck, Darmstadt, Germany), were diluted in experiments to a final concentration of 10, 20, or 50 μM, respectively. Control experiments were performed with an equal volume of DMSO.

After treatment for 5 or 24 h, cells were harvested and lysed with the double volume of RIPA buffer (50 mM Tris/HCl, pH 8.0, 150 mM NaCl, 0.5% sodium desoxycholate, 1% Triton X-100, 0.1% sodium dodecyl sulfate) supplemented with the protease inhibitor cocktail complete (Roche Diagnostics, Mannheim, Germany) and the phosphatase inhibitor cocktail PhosStop (Roche Diagnostics, Mannheim, Germany). After lysis, cell debris was removed by centrifugation. The protein content was determined according to a modified Bradford method (BioRad, Munich, Germany). Proteins were separated by sodium dodecyl sulfate polyacrylamide gel electrophoresis (two times for each cell line) and blotted onto polyvinylidene fluoride membranes. For each cell line, one membrane was incubated with a rabbit polyclonal antibody against total Akt (#9272, Cell Signaling Technology, Frankfurt, Germany) and the other with a rabbit monoclonal antibody recognizing phospho-S129-Akt (ab133458, Abcam, Berlin, Germany). Incubation with the primary antibodies was performed in a dilution 1:1000 in Tris-buffered saline (TBS, 20 mM Tris-HCl, pH 7.4, 150 mM NaCl) with 0.1% Tween-20 (TBS-T) and 5% bovine serum albumin for phospho-Akt or TBS-T with 5% nonfat dry milk for total Akt at 4 °C overnight. Then the membrane was washed twice for 10 min with TBS-T. Incubation with the peroxidase-coupled secondary anti-rabbit antibody followed for 1 h in the corresponding incubation buffer. The membrane was washed again twice for 10 min with TBS-T. Signals were developed and visualized by the SuperSignalTM West Pico Plus chemiluminescent substrate of Thermo Scientific (Rockford, USA).

Determination of a Protein Kinase Selectivity Profile of KN2. The screening service of Carna Bioscience, Inc., Kobe, Japan, was commissioned to determine a protein kinase selectivity profile of KN2. The company offers different representative subsets of the EPK superfamily for screening. We selected (i) the "tyrosine kinase (TK) panel", version 2.0, with 20 enzymes, (ii) the "serine/threonine kinase (STK) panel", version 3.0, with 30 enzymes, (iii) the "cell cycle panel", version 2.0, with 30 enzymes—among them the CK2α- and the CK2α'-based CK2 holoenzyme—involved in cell cycle control, and (iv) 11 individual EPKs for which significant off-target effects with certain CK2 inhibitors had been reported. The STK panel and the cell cycle panel are partly redundant so that on the whole 83 EPKs were used for the screening runs. All of them were applied as GST fusion constructs expressed in insect cells (baculovirus expression systems).

All EPK assays were performed in duplicate. The KN2 concentration was 3 μM in all assay mixtures. The ATP concentration for each kinase assay is given in Table S2; it was in the range of the K_M value of the respective kinase for ATP. The substrates for phosphorylation were EPK-specific peptides; the substrate concentration was 1 μM in all cases except PLK2, where it was 0.05 μM. For each EPK, the mean of the readout values of two control reactions (complete reaction mixture without inhibitor) was set as 0% inhibition, and the mean of the readout values of two background mixtures (without enzyme) was set as 100% inhibition; then, the percentage inhibition for each individual assay reaction was calculated. These values are visible in columns 4 and 5 of Table S2.

For a quantitative expression of selectivity, the Gini coefficients for 3 μM KN2, 10 μM TBI, and 1 μM 4,5,6,7-tetrabromo-1*H*-benzo[*d*][1,2,3]triazole were calculated as described by Graczyk[46] using a Microsoft Excel file provided in the Supporting Information of that publication. In the case of TBI and 4,5,6,7-tetrabromo-1*H*-benzo[*d*][1,2,3]triazole, the selectivity profile data published by Pagano *et al.*[45] were taken for this purpose.

Crystal Structure Determination and Illustration. The basis for determination of the CK2$\alpha'^{Cys336Ser}$/DPA and CK2$\alpha'^{Cys336Ser}$/KN2 complex structures of Table S1 is a procedure described recently.[35] Briefly, CK2$\alpha'^{Cys336Ser}$/MB002 cocrystals were grown in 28% (w/v) PEG 6000, 900 mM LiCl, 100 mM Tris/HCl, pH 8.5, optimized by micro- and macroseeding. The crystals were purged from unbound MB002, stabilized by dehydration, and finally subjected to extensive soaking in solutions with gradually increasing concentrations of the ligand of interest.

CK2α^{1-335} crystals for subsequent soaking experiments with KN2 were grown in 200 mM ammonium sulfate, 100 mM sodium cacodylate trihydrate, pH 6.5, and 30% (w/v) PEG 8000. Unlike CK2$\alpha'^{Cys336Ser}$, the crystallization additive MB002 was not added here. KN2 was soaked into either CK2α^{1-335} or CK2$\alpha'^{Cys336Ser}$ crystals by a stepwise increase of the ligand concentration. DPA was added simultaneously to some of the crystals with the intention to induce the unfolding of helix αD and thus to open the αD pocket and to facilitate the access and binding of KN2. The molar ratio of DPA to either CK2α^{1-335} or CK2$\alpha'^{Cys336Ser}$ in these crystallographic experiments was varied between 0.01:1 and 1000:1.

A C-terminally truncated CK1δ construct was prepared as described.[56] The recombinant protein was diluted with storage buffer to a concentration of 8 mg/mL. A 10 mM KN2 solution in DMSO was mixed in a 1:9 ratio with protein solution to give a final inhibitor concentration of 1 mM. After a 30 min incubation at ambient temperature, the solution was centrifuged to remove any precipitation. The clear supernatant was mixed in different ratios with reservoir solution G8 of the PEG/Ion HT crystal screen (Hampton Research), containing 2% (v/v) Tacsimate, pH 5.0, 100 mM sodium citrate tribasic dihydrate, pH 5.6, and 16% (w/v) PEG 3350. The crystallization was conducted using the sitting drop variant of vapor diffusion at a constant temperature of 20 °C.

All CK2$\alpha'^{Cys336Ser}$, CK2α^{1-335}, and CK1δ crystals were cryoprotected in the respective mother liquor plus 30% (v/v) ethylene glycol and finally flash-frozen in liquid nitrogen. X-ray diffraction data were collected at the synchrotron beamlines given in Tables S1 and S2. The data were collected at 100 K in all cases; the X-ray wavelengths are indicated in Tables S1 and S2.

The diffraction data were processed with the AUTOPROC toolbox (version 1.0.5)[57] using default settings. The pipeline applied XDS[58] for indexing and integration, POINTLESS[59] and AIMLESS[60] from the CCP4 suite[61] for symmetry determination and scaling, and finally STARANISO[62] for anisotropy analysis. The statistics in Tables S1 and S2 refer to the ellipsoidal data sets that were used for the further procedure.

https://doi.org/10.1021/acs.jmedchem.1c00063
J. Med. Chem. XXXX, XXX, XXX−XXX

The two CK2$\alpha'^{Cys336Ser}$ structures were solved *ab initio* with ARCIMBOLDO[63] followed by automated model building with the autobuild module of PHENIX.[64] The other structures were determined with molecular replacement using PHASER[65] within PHENIX[64] for search calculations. Chain A of a CK2α^{1-335} structure recently deposited at the PDB[66] (PDB_ID 6TEI)[38] and a CK1δ structure (PDB_ID 5MQV)[56] served as search models. All structures were optimized with several rounds of PHENIX refinement,[64] alternating with manual modeling using COOT.[67] The structural parametrization of the KN2 molecule was performed with the eLBOW module[68] of PHENIX,[64] whereas the parameters for MB002 and DPA were taken from the PDB[66] *via* COOT.[67]

The structures pictured in Figure 2, Figure 5a, and Figure S2 were prepared with PyMol.[69] The two-dimensional projection of KN2 binding to CK2$\alpha'^{Cys336Ser}$ in Figure 5b was generated with LigPlot+.[51] Movies S1 and S2 were produced with UCSF Chimera (version 1.15)[70] and the open source cross platform video editor Shotcut (version 19.04.30).

■ ASSOCIATED CONTENT

Supporting Information

The Supporting Information is available free of charge at https://pubs.acs.org/doi/10.1021/acs.jmedchem.1c00063.

Figures S1−S8 with CK2α/CK2α' sequence alignment, CK1δ/KN2 crystal structure, dose−response curve for the CK1ε inhibition by KN2, ^{1}H NMR spectra of compound **1** and KN2, HPLC chromatogram of KN2, ^{13}C NMR spectrum of KN2, and HRMS spectrum of KN2; Tables S1 and S2 with X-ray diffraction data and refinement statistics; Table S3 with selectivity profiling data (PDF)

Movies S1 and S2 illustrating the local mobility of the helix αD region of crystalline CK2α' upon binding of DPA and KN2, respectively (MP4, MP4)

SMILES molecular formula strings and K_i values (CSV)

Atomic coordinates and experimental structure factors of the three CK2α/CK2α' structures in Table S1 (PDB, CIF, PDB, CIF, PDB, CIF)

Accession Codes

The PDB codes of the three crystal structures (Table S1) are 7AT9 (CK2$\alpha'^{Cys336Ser}$/DPA/MB002), 7ATV (CK2$\alpha'^{Cys336Ser}$/KN2), and 7AT5 (CK2α^{1-335}/KN2).

■ AUTHOR INFORMATION

Corresponding Author

Karsten Niefind − *Department für Chemie, Institut für Biochemie, Universität zu Köln, D-50674 Köln, Germany;* orcid.org/0000-0002-0183-6315; Phone: +49-221-470-6444; Email: Karsten.Niefind@uni-koeln.de; Fax: +49-221-470-3244

Authors

Dirk Lindenblatt − *Department für Chemie, Institut für Biochemie, Universität zu Köln, D-50674 Köln, Germany;* orcid.org/0000-0002-5561-1082

Violetta Applegate − *Department für Chemie, Institut für Biochemie, Universität zu Köln, D-50674 Köln, Germany;* orcid.org/0000-0003-4120-7983

Anna Nickelsen − *Institut für Pharmazeutische und Medizinische Chemie, Westfälische Wilhelms-Universität Münster, D-48149 Münster, Germany;* orcid.org/0000-0001-9887-6403

Merlin Klußmann − *Department für Chemie, Institut für Biochemie, Universität zu Köln, D-50674 Köln, Germany;* orcid.org/0000-0001-6041-0501

Ines Neundorf − *Department für Chemie, Institut für Biochemie, Universität zu Köln, D-50674 Köln, Germany;* orcid.org/0000-0001-6450-3991

Claudia Götz − *Medizinische Biochemie und Molekularbiologie, Universität des Saarlandes, D-66421 Homburg/Saar, Germany;* orcid.org/0000-0001-7115-0485

Joachim Jose − *Institut für Pharmazeutische und Medizinische Chemie, Westfälische Wilhelms-Universität Münster, D-48149 Münster, Germany;* orcid.org/0000-0002-0666-2676

Complete contact information is available at: https://pubs.acs.org/10.1021/acs.jmedchem.1c00063

Notes

The authors declare no competing financial interest.

■ ACKNOWLEDGMENTS

We thank Professor Ulrich Baumann (University of Cologne) for a CK1δ expression strain and for access to protein crystallography infrastructure (c2f.uni-koeln.de), Professor Maria Bretner (Warsaw Technical University) for MB002 and TBIa, Dr. Jörg Fabian (University of Münster) for HRMS measurement and Dr. Jens Köhler (University of Münster) for NMR spectroscopy with KN2. We are grateful to the staff of the European Synchrotron Radiation Facility (ESRF), of the Helmholtz-Zentrum Berlin and of the European Molecular Biology Laboratory (EMBL) at DESY for assistance with diffraction data collection. The work was funded by the Deutsche Forschungsgemeinschaft (DFG; Grant NI 643/4-2).

■ ABBREVIATIONS

CK1δ, casein kinase 1, isoform δ; CK1ε, casein kinase 1, isoform ε; CK2, casein kinase 2; CK2α, catalytic subunit of protein kinase CK2; CK2α', paralogous isoform of CK2α; CK2β, regulatory subunit of protein kinase CK2; PDB, Protein Data Bank

■ REFERENCES

(1) Yesudhas, D.; Srivastava, A.; Gromiha, M. M. COVID-19 outbreak: history, mechanism, transmission, structural studies and therapeutics. *Infection* **2021**, *49*, 199−213.

(2) Bouhaddou, M.; Memon, D.; Meyer, B.; White, K. M.; Rezelj, V. V.; Correa Marrero, M.; Polacco, B. J.; Melnyk, J. E.; Ulferts, S.; Kaake, R. M.; Batra, J.; Richards, A. L.; Stevenson, E.; Gordon, D. E.; Rojc, A.; Obernier, K.; Fabius, J. M.; Soucheray, M.; Miorin, L.; Moreno, E.; Koh, C.; Tran, Q. D.; Hardy, A.; Robinot, R.; Vallet, T.; Nilsson-Payant, B. E.; Hernandez-Armenta, C.; Dunham, A.; Weigang, S.; Knerr, J.; Modak, M.; Quintero, D.; Zhou, Y.; Dugourd, A.; Valdeolivas, A.; Patil, T.; Li, Q.; Hüttenhain, R.; Cakir, M.; Muralidharan, M.; Kim, M.; Jang, G.; Tutuncuoglu, B.; Hiatt, J.; Guo, J. Z.; Xu, J.; Bouhaddou, S.; Mathy, C. J. P.; Gaulton, A.; Manners, E. J.; Félix, E.; Shi, Y.; Goff, M.; Lim, J. K.; McBride, T.; O'Neal, M. C.; Cai, Y.; Chang, J. C. J.; Broadhurst, D. J.; Klippsten, S.; De Wit, E.; Leach, A. R.; Kortemme, T.; Shoichet, B.; Ott, M.; Saez-Rodriguez, J.; tenOever, B. R.; Mullins, R. D.; Fischer, E. R.; Kochs, G.; Grosse, R.; García-Sastre, A.; Vignuzzi, M.; Johnson, J. R.; Shokat, K. M.; Swaney, D. L.; Beltrao, P.; Krogan, N. J. The global phosphorylation landscape of SARS-CoV-2 infection. *Cell* **2020**, *182*, 685−712.

(3) Cruz, L. R.; Baladrón, I.; Rittoles, A.; Díaz, P. A.; Valenzuela, C.; Santana, R.; Vázquez, M. M.; García, A.; Chacón, D.; Thompson, D.; Perera, G.; González, A.; Reyes, R.; Torres, L.; Pérez, J.; Valido, Y.; Rodriguez, R.; Vázquez-Bloomquist, D. M.; Rosales, M.; Ramón, A. C.; Pérez, G. V.; Guillén, G.; Muzio, V.; Perera, Y.; Perea, S. E. Treatment with an anti-CK2 synthetic peptide improves clinical response in COVID-19 patients with pneumonia. A randomized and controlled clinical trial. *ACS Pharmacol Transl Sci.* **2021**, *4*, 206−212.
(4) Siddiqui-Jain, A.; Drygin, D.; Streiner, N.; Chua, P.; Pierre, F.; O'Brien, S. E.; Bliesath, J.; Omori, M.; Huser, N.; Ho, C.; Proffitt, C.; Schwaebe, M. K.; Ryckman, D. M.; Rice, W. G.; Anderes, K. CX-4945, an orally bioavailable selective inhibitor of protein kinase CK2, inhibits prosurvival and angiogenic signaling and exhibits antitumor efficacy. *Cancer Res.* **2010**, *70*, 10288−10298.
(5) Silmitasertib (CX-4945) in Patients With Severe Coronavirus Disease 2019 (COVID-19) (CX4945); https://clinicaltrials.gov/ct2/show/NCT04668209 (accessed July 23, 2021).
(6) Study of CX-4945 in Combination With Gemcitabine and Cisplatin for Frontline Treatment of Cholangiocarcinom; https://clinicaltrials.gov/ct2/show/NCT02128282 (accessed July 23, 2021).
(7) Ruzzene, M.; Pinna, L. A. Addiction to protein kinase CK2: a common denominator of diverse cancer cells? *Biochim. Biophys. Acta, Proteins Proteomics* **2010**, *1804*, 499−504.
(8) Di Maira, G.; Salvi, M.; Arrigoni, G.; Marin, O.; Sarno, S.; Brustolon, F.; Pinna, L. A.; Ruzzene, M. Protein kinase CK2 phosphorylates and upregulates Akt/PKB. *Cell Death Differ.* **2005**, *12*, 668−677.
(9) Purzner, T.; Purzner, J.; Buckstaff, T.; Cozza, G.; Gholamin, S.; Rusert, J. M.; Hartl, T. A.; Sanders, J.; Conley, N.; Ge, X.; Langan, M.; Ramaswamy, V.; Ellis, L.; Litzenburger, U.; Bolin, S.; Theruvath, J.; Nitta, R.; Qi, L.; Li, X. N.; Li, G.; Taylor, M. D.; Wechsler-Reya, R. J.; Pinna, L. A.; Cho, Y. J.; Fuller, M. T.; Elias, J. E.; Scott, M. P. Developmental phosphoproteomics identifies the kinase CK2 as a driver of Hedgehog signaling and a therapeutic target in medulloblastoma. *Sci. Signaling* **2018**, *11*, No. eaau5147.
(10) Duncan, J. S.; Turowec, J. P.; Duncan, K. E.; Vilk, G.; Wu, C.; Lüscher, B.; Li, S. S.; Gloor, G. B.; Litchfield, D. W. A peptide-based target screen implicates the protein kinase CK2 in the global regulation of caspase signaling. *Sci. Signaling* **2011**, *4*, No. ra30.
(11) Battistutta, R.; Cozza, G.; Pierre, F.; Papinutto, E.; Lolli, G.; Sarno, S.; O'Brien, S. E.; Siddiqui-Jain, A.; Haddach, M.; Anderes, K.; Ryckman, D. M.; Meggio, F.; Pinna, L. A. Unprecedented selectivity and structural determinants of a new class of protein kinase CK2 inhibitors in clinical trials for the treatment of cancer. *Biochemistry* **2011**, *50*, 8478−8488.
(12) Oshima, T.; Niwa, Y.; Kuwata, K.; Srivastava, A.; Hyoda, T.; Tsuchiya, Y.; Kumagai, M.; Tsuyuguchi, M.; Tamaru, T.; Sugiyama, A.; Ono, N.; Zolboot, N.; Aikawa, Y.; Oishi, S.; Nonami, A.; Arai, F.; Hagihara, S.; Yamaguchi, J.; Tama, F.; Kunisaki, Y.; Yagita, K.; Ikeda, M.; Kinoshita, T.; Kay, S. A.; Itami, K.; Hirota, T. Cell-based screen identifies a new potent and highly selective CK2 inhibitor for modulation of circadian rhythms and cancer cell growth. *Sci. Adv.* **2019**, *5*, No. eaau9060.
(13) Dowling, J. E.; Alimzhanov, M.; Bao, L.; Chuaqui, C.; Denz, C. R.; Jenkins, E.; Larsen, N. A.; Lyne, P. D.; Pontz, T.; Ye, Q.; Holdgate, G. A.; Snow, L.; O'Connell, N.; Ferguson, A. Potent and selective CK2 kinase inhibitors with effects on Wnt pathway signaling *in vivo*. *ACS Med. Chem. Lett.* **2016**, *7*, 300−5.
(14) Hashimoto, A.; Gao, C.; Mastio, J.; Kossenkov, A.; Abrams, S. I.; Purandare, A. V.; Desilva, H.; Wee, S.; Hunt, J.; Jure-Kunkel, M.; Gabrilovich, D. I. Inhibition of casein kinase 2 disrupts differentiation of myeloid cells in cancer and enhances the efficacy of immunotherapy in mice. *Cancer Res.* **2018**, *78*, 5644−5655.
(15) Roskoski, R. Classification of small molecule protein kinase inhibitors based upon the structures of their drug-enzyme complexes. *Pharmacol. Res.* **2016**, *103*, 26−48.
(16) Taylor, S. S.; Kornev, A. P. Protein kinases: evolution of dynamic regulatory proteins. *Trends Biochem. Sci.* **2011**, *36*, 65−77.
(17) Niefind, K.; Raaf, J.; Issinger, O. G. Protein kinase CK2 in health and disease: Protein kinase CK2: from structures to insights. *Cell. Mol. Life Sci.* **2009**, *66*, 1800−1816.
(18) Chen, X.; Li, C.; Wang, D.; Chen, Y.; Zhang, N. Recent advances in the discovery of CK2 allosteric inhibitors: from traditional screening to structure-based design. *Molecules* **2020**, *25*, 870.
(19) Lamba, V.; Ghosh, I. New directions in targeting protein kinases: focusing upon true allosteric and bivalent inhibitors. *Curr. Pharm. Des.* **2012**, *18*, 2936−2945.
(20) Pietsch, M.; Viht, K.; Schnitzler, A.; Ekambaram, R.; Steinkrüger, M.; Enkvist, E.; Nienberg, C.; Nickelsen, A.; Lauwers, M.; Jose, J.; Uri, A.; Niefind, K. Unexpected CK2β-antagonistic functionality of bisubstrate inhibitors targeting protein kinase CK2. *Bioorg. Chem.* **2020**, *96*, 103608.
(21) Rahnel, H.; Viht, K.; Lavogina, D.; Mazina, O.; Haljasorg, T.; Enkvist, E.; Uri, A. A selective biligand inhibitor of CK2 increases caspase-3 activity in cancer cells and inhibits platelet aggregation. *ChemMedChem* **2017**, *12*, 1723−1736.
(22) Viht, K.; Saaver, S.; Vahter, J.; Enkvist, E.; Lavogina, D.; Sinijärv, H.; Raidaru, G.; Guerra, B.; Issinger, O. G.; Uri, A. Acetoxymethyl ester of tetrabromobenzimidazole-peptoid conjugate for inhibition of protein kinase CK2 in living cells. *Bioconjugate Chem.* **2015**, *26*, 2324−35.
(23) Enkvist, E.; Viht, K.; Bischoff, N.; Vahter, J.; Saaver, S.; Raidaru, G.; Issinger, O. G.; Niefind, K.; Uri, A. A subnanomolar fluorescent probe for protein kinase CK2 interaction studies. *Org. Biomol. Chem.* **2012**, *10*, 8645−8653.
(24) De Fusco, C.; Brear, P.; Iegre, J.; Georgiou, K. H.; Sore, H. F.; Hyvönen, M.; Spring, D. R. A fragment-based approach leading to the discovery of a novel binding site and the selective CK2 inhibitor CAM4066. *Bioorg. Med. Chem.* **2017**, *25*, 3471−3482.
(25) Brear, P.; De Fusco, C.; Hadje Georgiou, K.; Francis-Newton, N. J.; Stubbs, C. J.; Sore, H. F.; Venkitaraman, A. R.; Abell, C.; Spring, D. R.; Hyvonen, M. Specific inhibition of CK2α from an anchor outside the active site. *Chem. Sci.* **2016**, *7*, 6839−6845.
(26) Gower, C. M.; Chang, M. E.; Maly, D. J. Bivalent inhibitors of protein kinases. *Crit. Rev. Biochem. Mol. Biol.* **2014**, *49*, 102−15.
(27) Atkinson, E. L.; Iegre, J.; Brear, P. D.; Zhabina, E. A.; Hyvönen, M.; Spring, D. R. Downfalls of chemical probes acting at the kinase ATP-site: CK2 as a case study. *Molecules* **2021**, *26*, 1977.
(28) Niefind, K.; Guerra, B.; Ermakowa, I.; Issinger, O. Crystal structure of human protein kinase CK2: insights into basic properties of the CK2 holoenzyme. *EMBO J.* **2001**, *20*, 5320−5331.
(29) Iegre, J.; Brear, P.; Baker, D. J.; Tan, Y. S.; Atkinson, E. L.; Sore, H. F.; O'Donovan, D. H.; Verma, C. S.; Hyvönen, M.; Spring, D. R. Efficient development of stable and highly functionalised peptides targeting the CK2α/CK2β protein-protein interaction. *Chem. Sci.* **2019**, *10*, 5056−5063.
(30) Kufareva, I.; Bestgen, B.; Brear, P.; Prudent, R.; Laudet, B.; Moucadel, V.; Ettaoussi, M.; Sautel, C. F.; Krimm, I.; Engel, M.; Filhol, O.; Borgne, M. L.; Lomberget, T.; Cochet, C.; Abagyan, R. Discovery of holoenzyme-disrupting chemicals as substrate-selective CK2 inhibitors. *Sci. Rep.* **2019**, *9*, 15893.
(31) Brear, P.; North, A.; Iegre, J.; Hadje Georgiou, K.; Lubin, A.; Carro, L.; Green, W.; Sore, H. F.; Hyvönen, M.; Spring, D. R. Novel non-ATP competitive small molecules targeting the CK2 α/β interface. *Bioorg. Med. Chem.* **2018**, *26*, 3016−3020.
(32) Lindenblatt, D.; Horn, M.; Götz, C.; Niefind, K.; Neundorf, I.; Pietsch, M. Design of CK2β-mimicking peptides as tools to study the CK2α/CK2β interaction in cancer cells. *ChemMedChem* **2019**, *14*, 833−841.
(33) Raaf, J.; Guerra, B.; Neundorf, I.; Bopp, B.; Issinger, O. G.; Jose, J.; Pietsch, M.; Niefind, K. First structure of protein kinase CK2 catalytic subunit with an effective CK2β-competitive ligand. *ACS Chem. Biol.* **2013**, *8*, 901−907.
(34) Bischoff, N.; Olsen, B.; Raaf, J.; Bretner, M.; Issinger, O. G.; Niefind, K. Structure of the human protein kinase CK2 catalytic subunit CK2α' and interaction thermodynamics with the regulatory subunit CK2β. *J. Mol. Biol.* **2011**, *407*, 1−12.

https://doi.org/10.1021/acs.jmedchem.1c00063
J. Med. Chem. XXXX, XXX, XXX−XXX

(35) Lindenblatt, D.; Nickelsen, A.; Applegate, V. M.; Hochscherf, J.; Witulski, B.; Bouaziz, Z.; Marminon, C.; Bretner, M.; Le Borgne, M.; Jose, J.; Niefind, K. Diacritic binding of an indenoindole inhibitor by CK2α paralogs explored by a reliable path to atomic resolution CK2α' structures. *ACS Omega* **2019**, *4*, 5471−5478.
(36) Raaf, J.; Klopffleisch, K.; Issinger, O.; Niefind, K. The catalytic subunit of human protein kinase CK2 structurally deviates from its maize homologue in complex with the nucleotide competitive inhibitor emodin. *J. Mol. Biol.* **2008**, *377*, 1−8.
(37) Ermakova, I.; Boldyreff, B.; Issinger, O.; Niefind, K. Crystal structure of a C-terminal deletion mutant of human protein kinase CK2 catalytic subunit. *J. Mol. Biol.* **2003**, *330*, 925−934.
(38) Lindenblatt, D.; Nickelsen, A.; Applegate, V. M.; Jose, J.; Niefind, K. Structural and mechanistic basis of the inhibitory potency of selected 2-aminothiazole compounds on protein kinase CK2. *J. Med. Chem.* **2020**, *63*, 7766−7772.
(39) Chojnacki, K.; Lindenblatt, D.; Wińska, P.; Wielechowska, M.; Toelzer, C.; Niefind, K.; Bretner, M. Synthesis, biological properties and structural study of new halogenated azolo[4,5-*b*]pyridines as inhibitors of CK2 kinase. *Bioorg. Chem.* **2021**, *106*, 104502.
(40) Bestgen, B.; Krimm, I.; Kufareva, I.; Kamal, A. A. M.; Seetoh, W. G.; Abell, C.; Hartmann, R. W.; Abagyan, R.; Cochet, C.; Le Borgne, M.; Engel, M.; Lomberget, T. 2-aminothiazole derivatives as selective allosteric modulators of the protein kinase CK2. 1. Identification of an allosteric binding site. *J. Med. Chem.* **2019**, *62*, 1803−1816.
(41) Chojnacki, K.; Wińska, P.; Wielechowska, M.; Łukowska-Chojnacka, E.; Tölzer, C.; Niefind, K.; Bretner, M. Biological properties and structural study of new aminoalkyl derivatives of benzimidazole and benzotriazole, dual inhibitors of CK2 and PIM1 kinases. *Bioorg. Chem.* **2018**, *80*, 266−275.
(42) Palm, K.; Luthman, K.; Ungell, A. L.; Strandlund, G.; Beigi, F.; Lundahl, P.; Artursson, P. Evaluation of dynamic polar molecular surface area as predictor of drug absorption: comparison with other computational and experimental predictors. *J. Med. Chem.* **1998**, *41*, 5382−5392.
(43) Lipinski, C. A.; Lombardo, F.; Dominy, B. W.; Feeney, P. J. Experimental and computational approaches to estimate solubility and permeability in drug discovery and development settings. *Adv. Drug Delivery Rev.* **2001**, *46*, 3−26.
(44) Pierre, F.; Chua, P. C.; O'Brien, S. E.; Siddiqui-Jain, A.; Bourbon, P.; Haddach, M.; Michaux, J.; Nagasawa, J.; Schwaebe, M. K.; Stefan, E.; Vialettes, A.; Whitten, J. P.; Chen, T. K.; Darjania, L.; Stansfield, R.; Anderes, K.; Bliesath, J.; Drygin, D.; Ho, C.; Omori, M.; Proffitt, C.; Streiner, N.; Trent, K.; Rice, W. G.; Ryckman, D. M. Discovery and SAR of 5-(3-chlorophenylamino)benzo[*c*][2,6]-naphthyridine-8-carboxylic acid (CX-4945), the first clinical stage inhibitor of protein kinase CK2 for the treatment of cancer. *J. Med. Chem.* **2011**, *54*, 635−654.
(45) Pagano, M. A.; Bain, J.; Kazimierczuk, Z.; Sarno, S.; Ruzzene, M.; Di Maira, G.; Elliott, M.; Orzeszko, A.; Cozza, G.; Meggio, F.; Pinna, L. A. The selectivity of inhibitors of protein kinase CK2: an update. *Biochem. J.* **2008**, *415*, 353−365.
(46) Graczyk, P. P. Gini coefficient: a new way to express selectivity of kinase inhibitors against a family of kinases. *J. Med. Chem.* **2007**, *50*, 5773−5779.
(47) Ursu, A.; Childs-Disney, J. L.; Angelbello, A. J.; Costales, M. G.; Meyer, S. M.; Disney, M. D. Gini coefficients as a single value metric to define chemical probe selectivity. *ACS Chem. Biol.* **2020**, *15*, 2031−2040.
(48) Battistutta, R.; Mazzorana, M.; Sarno, S.; Kazimierczuk, Z.; Zanotti, G.; Pinna, L. A. Inspecting the structure-activity relationship of protein kinase CK2 inhibitors derived from tetrabromo-benzimidazole. *Chem. Biol.* **2005**, *12*, 1211−1219.
(49) Janeczko, M.; Orzeszko, A.; Kazimierczuk, Z.; Szyszka, R.; Baier, A. CK2α and CK2α' subunits differ in their sensitivity to 4,5,6,7-tetrabromo- and 4,5,6,7-tetraiodo-1*H*-benzimidazole derivatives. *Eur. J. Med. Chem.* **2012**, *47*, 345−350.
(50) Bollacke, A.; Nienberg, C.; Le Borgne, M.; Jose, J. Toward selective CK2α and CK2α inhibitors: development of a novel whole-cell kinase assay by Autodisplay of catalytic CK2α'. *J. Pharm. Biomed. Anal.* **2016**, *121*, 253−260.
(51) Laskowski, R. A.; Swindells, M. B. LigPlot+: multiple ligand-protein interaction diagrams for drug discovery. *J. Chem. Inf. Model.* **2011**, *51*, 2778−2786.
(52) Najda-Bernatowicz, A.; Łebska, M.; Orzeszko, A.; Kopańska, K.; Krzywińska, E.; Muszyńska, G.; Bretner, M. Synthesis of new analogs of benzotriazole, benzimidazole and phthalimide - potential inhibitors of human protein kinase CK2. *Bioorg. Med. Chem.* **2009**, *17*, 1573−1578.
(53) Bischoff, N.; Raaf, J.; Olsen, B.; Bretner, M.; Issinger, O.; Niefind, K. Enzymatic activity with an incomplete catalytic spine: insights from a comparative structural analysis of human CK2α and its paralogous isoform CK2α'. *Mol. Cell. Biochem.* **2011**, *356*, 57−65.
(54) Gratz, A.; Götz, C.; Jose, J. A CE-based assay for human protein kinase CK2 activity measurement and inhibitor screening. *Electrophoresis* **2010**, *31*, 634−640.
(55) Copeland, R. A. *Enzymes: A practical introduction to structure, mechanism, and data analysis*, 2nd ed.; Wiley-VCH: New York, 2000.
(56) Halekotte, J.; Witt, L.; Ianes, C.; Krüger, M.; Bührmann, M.; Rauh, D.; Pichlo, C.; Brunstein, E.; Luxenburger, A.; Baumann, U.; Knippschild, U.; Bischof, J.; Peifer, C. Optimized 4,5-diarylimidazoles as potent/selective inhibitors of protein kinase CK1δ and their structural relation to p38α MAPK. *Molecules* **2017**, *22*, 522.
(57) Vonrhein, C.; Flensburg, C.; Keller, P.; Sharff, A.; Smart, O.; Paciorek, W.; Womack, T.; Bricogne, G. Data processing and analysis with the autoPROC toolbox. *Acta Crystallogr., Sect. D: Biol. Crystallogr.* **2011**, *67*, 293−302.
(58) Kabsch, W. XDS. *Acta Crystallogr., Sect. D: Biol. Crystallogr.* **2010**, *66*, 125−132.
(59) Evans, P. Scaling and assessment of data quality. *Acta Crystallogr., Sect. D: Biol. Crystallogr.* **2006**, *62*, 72−82.
(60) Evans, P. R.; Murshudov, G. N. How good are my data and what is the resolution? *Acta Crystallogr., Sect. D: Biol. Crystallogr.* **2013**, *69*, 1204−12014.
(61) Winn, M. D.; Ballard, C. C.; Cowtan, K. D.; Dodson, E. J.; Emsley, P.; Evans, P. R.; Keegan, R. M.; Krissinel, E. B.; Leslie, A. G.; McCoy, A.; McNicholas, S. J.; Murshudov, G. N.; Pannu, N. S.; Potterton, E. A.; Powell, H. R.; Read, R. J.; Vagin, A.; Wilson, K. S. Overview of the CCP4 suite and current developments. *Acta Crystallogr., Sect. D: Biol. Crystallogr.* **2011**, *67*, 235−242.
(62) Tickle, I. J.; Flensburg, C.; Keller, P.; Paciorek, W.; Sharff, A.; Vonrhein, C.; Bricogne, G. *STARANISO*; Global Phasing Ltd.: Cambridge, U.K., 2018.
(63) Rodríguez, D. D.; Grosse, C.; Himmel, S.; González, C.; de Ilarduya, I. M.; Becker, S.; Sheldrick, G. M.; Usón, I. Crystallographic *ab initio* protein structure solution below atomic resolution. *Nat. Methods* **2009**, *6*, 651−653.
(64) Adams, P. D.; Afonine, P. V.; Bunkóczi, G.; Chen, V. B.; Davis, I. W.; Echols, N.; Headd, J. J.; Hung, L. W.; Kapral, G. J.; Grosse-Kunstleve, R. W.; McCoy, A. J.; Moriarty, N. W.; Oeffner, R.; Read, R. J.; Richardson, D. C.; Richardson, J. S.; Terwilliger, T. C.; Zwart, P. H. PHENIX: a comprehensive Python-based system for macromolecular structure solution. *Acta Crystallogr., Sect. D: Biol. Crystallogr.* **2010**, *66*, 213−221.
(65) McCoy, A. J.; Grosse-Kunstleve, R. W.; Adams, P. D.; Winn, M. D.; Storoni, L. C.; Read, R. J. Phaser crystallographic software. *J. Appl. Crystallogr.* **2007**, *40*, 658−674.
(66) Berman, H. M.; Westbrook, J.; Feng, Z.; Gilliland, G.; Bhat, T. N.; Weissig, H.; Shindyalov, I. N.; Bourne, P. E. The protein data bank. *Nucleic Acids Res.* **2000**, *28*, 235−242.
(67) Emsley, P.; Lohkamp, B.; Scott, W. G.; Cowtan, K. Features and development of Coot. *Acta Crystallogr., Sect. D: Biol. Crystallogr.* **2010**, *66*, 486−501.
(68) Moriarty, N. W.; Grosse-Kunstleve, R. W.; Adams, P. D. electronic Ligand Builder and Optimization Workbench (eLBOW): a

https://doi.org/10.1021/acs.jmedchem.1c00063
J. Med. Chem. XXXX, XXX, XXX−XXX

tool for ligand coordinate and restraint generation. *Acta Crystallogr., Sect. D: Biol. Crystallogr.* **2009**, *65*, 1074−1080.
(69) *The PyMOL Molecular Graphics System*, version 1.7; Schrödinger, LLC, 2013.
(70) Pettersen, E. F.; Goddard, T. D.; Huang, C. C.; Couch, G. S.; Greenblatt, D. M.; Meng, E. C.; Ferrin, T. E. UCSF Chimera - a visualization system for exploratory research and analysis. *J. Comput. Chem.* **2004**, *25*, 1605−1612.

https://doi.org/10.1021/acs.jmedchem.1c00063
J. Med. Chem. XXXX, XXX, XXX−XXX